J Mater Sci (2010) 45:725–732
DOI 10.1007/s10853-009-3991-9

A comparative study of different solvothermal methods for the synthesis of Sn^{2+}-doped $BaTiO_3$ powders and their dielectric properties

Yahong Xie · Shu Yin · Takatoshi Hashimoto · Yuichi Tokano · Atsushi Sasaki · Tsugio Sato

Received: 23 April 2009 / Accepted: 23 October 2009 / Published online: 5 November 2009

Abstract Ternary oxides containing Sn^{2+} are rare and difficult to prepare by the conventional solid state reactions due to the disproportionation of Sn^{2+} to Sn^{4+} and Sn at high temperatures. In this article, Sn^{2+}-doped barium titanate, $Ba_{1-x}Sn_xTiO_3$ ($x = 0.00, 0.02, 0.05$, and 0.10) nanopowders were successfully synthesized at a moderate temperature by a microwave-assisted solvothermal reaction (MSR) and a solvothermal reaction with rolling (SRR). The powders obtained using the MSR and SRR consisted of nanoparticles of 20–50 nm and 100–120 nm in diameter, respectively. The dielectric constant of the sample increased by doping with a small amount of Sn^{2+} ($x \leq 0.05$), but decreased by doping in excess amounts of it.

Introduction

Transition metal oxides containing Sn^{2+} show some unique properties such as being visible light responsive photocatalytic, piezoelectric, etc. However, the formation of Sn^{2+}-containing compound by a conventional solid state reaction is difficult due to the disproportionation of Sn^{2+} to Sn^{4+} and Sn at high temperature [1–5] and only several compounds such as $SnWO_6$ [6], $SnNb_2O_6$ [7], Sn_2TiO_4 [8], and some pyrochlore compounds [1, 9] have been reported. In a previous article [10], we succeeded in preparing Sn^{2+}-doped barium titanate for the first time by a microwave-assisted solvothermal reaction under moderate reaction conditions such as 200 °C for 1 h to avoid the disproportionation reaction of Sn^{2+} at high temperatures.

Barium titanate ($BaTiO_3$) is a well-known lead-free dielectric and piezoelectric material [11–14]. It is well known that the dielectric and piezoelectric properties of $BaTiO_3$ change by doping with metal ions such as Sr^{2+}, Ca^{2+}, etc., and it may be expected that the dielectric and piezoelectric properties of $BaTiO_3$ can be modified by doping with a Sn^{2+} possessing lone-pair-electron-like Pb^{2+} [15, 16]. Therefore, in this article, a microwave-assisted solvothermal reaction (MSR) [17] and a solvothermal reaction with rolling (SRR) [18] were implemented in an attempt to synthesize a single phase of perovskite-type Sn^{2+}-doped $BaTiO_3$, $Ba_{1-x}Sn_xTiO_3$ ($x = 0.00$, 0.02, 0.05, and 0.10) under mild reaction conditions.

Experimental

Synthesis techniques

Reagent grade $BaCl_2$, $SnCl_2{\cdot}2H_2O$, and $Ti(i\text{-}C_3H_7O)_4$ were used as starting materials. Initially, a $SnCl_2$–$BaCl_2$ mixed aqueous solution and a $Ti(i\text{-}C_3H_7O)_4$ i-propanol solution were mixed under stirring, where the molar ratio of (Sn + Ba)/Ti was fixed at 1:1. KOH was added into the solution as a mineralizer. Then, the suspended solution was diluted with water to adjust the concentrations of $Sn^{2+} + Ba^{2+}$, Ti^{4+}, and KOH to 0.2, 0.2, and 2.0 M, respectively, and treated via two different routes.

Y. Xie (✉) · S. Yin · T. Sato
Institute of Multidisciplinary Research for Advanced Materials (IMRAM), Tohoku University, Sendai 980-8577, Japan
e-mail: xyh0707@hotmail.com

T. Hashimoto · Y. Tokano · A. Sasaki
NEC Tokin Corporation, Koriyama, Taihaku-ku, Sendai 980-8510, Japan

Microwave-assisted solvothermal reaction

The solution of 40 cm^3 was transferred to a Teflon®-lined reaction vessel with 70 cm^3 of internal volume and then was irradiated by microwaves to start the solvothermal reaction at 200 °C for 1 h using a microwave reaction apparatus (ACTAC Co., MWS-2).

Solvothermal reaction with rolling

The solution of 70 cm^3 was transferred to a Teflon®-lined stainless steel vessel with 100 cm^3 of internal volume and 5.5 cm in outer diameter with 10 Teflon® balls of 1.1 cm in diameter. Then, the vessel was sealed and heated at 200 °C for 12 h in an electric oven, where the vessel was rotated at 100 rpm during the reaction.

After the reaction, the precipitates obtained by both the methods were collected with a centrifuge and rinsed with ethanol, deionized water, and acetone for three times, respectively, and dried overnight at 60 °C in a vacuum oven.

Characterization

Thermogravimetric analysis (TG-DTA, Rigaku, TG8101D) was performed for the powders from room temperature up to 1200 °C with a heating rate of 10 °C/min in air. The particle morphology was observed using a transmission electron microscope (JEOL, JEM-2000EX). The X-ray diffraction (XRD) analysis of the obtained powder samples was carried out using CuKα radiation with a pyrolytic graphite monochromator mounted on a powder diffractometer (Shimadzu XD-D1).

After adding 0.1-wt% Li_2CO_3 and 0.5-wt% V_2O_5 as sintering aid, the powders were uniaxially pressed at 20 MPa in a steel die to form pellets of x mm in diameter and y mm thick and then isostatically pressed at 200 MPa. The pellets were then sintered at 1200 °C for 5 h. The morphologies of the sintered bodies were observed for the polished surfaces after thermal etching at 1150 °C for 1 h by a scanning electron microscope (SEM. Hitachi S-4100). The densities of the sintered pellets were measured by Archimedes' methods. The dielectric constants were determined using an Agilent 4294A precision impedance analyzer.

Results and discussion

Thermal decomposition process

Figures 1 and 2 show the TG-DTA curves of the $Ba_{1-x}Sn_xTiO_3$ ($x = 0.00$, 0.02, 0.05, and 0.10) samples obtained

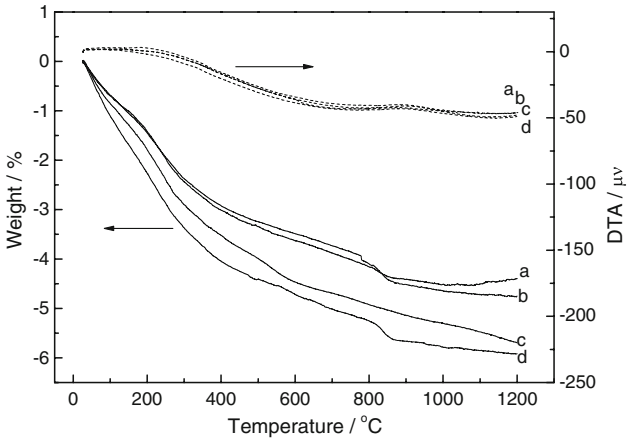

Fig. 1 TG-DTA curves for the (*a*) $BaTiO_3$, (*b*) $Ba_{0.98}Sn_{0.02}TiO_3$, (*c*) $Ba_{0.95}Sn_{0.05}TiO_3$, (*d*) $Ba_{0.90}Sn_{0.10}TiO_3$ powders as prepared by MSR at 200 °C for 1 h in 2-M KOH aqueous solutions

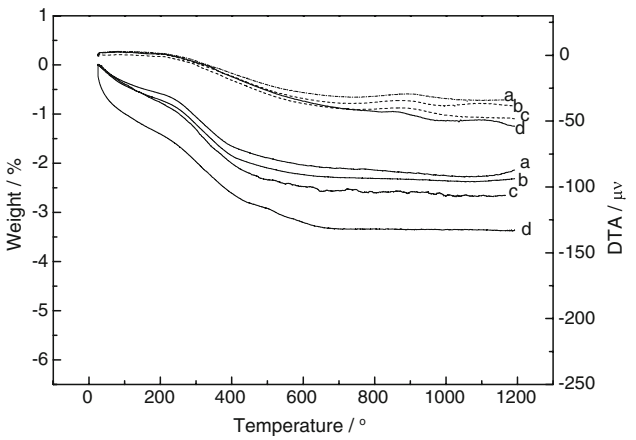

Fig. 2 TG-DTA curves for the (*a*) $BaTiO_3$, (*b*) $Ba_{0.98}Sn_{0.02}TiO_3$, (*c*) $Ba_{0.95}Sn_{0.05}TiO_3$, (*d*) $Ba_{0.90}Sn_{0.10}TiO_3$ powders as prepared by SRR at 200 °C for 12 h in 2-M KOH aqueous solutions

at 200 °C for 1 h by MSR, and at 200 °C for 12 h by SRR, respectively. All samples showed weight loss to some extent until 1000 °C and then the weights were almost constant. The weight loss in the temperature range from room temperature to 200, 200–800, and above 800 °C might be attributed to the release of physisorbed water, the dehydration of hydroxyl groups in the lattice, and release of CO_2 coming from the decomposition of $BaCO_3$ which might be formed by the reaction of Ba^{2+} in the solution and CO_2 in air during the treatment of the reaction solution, respectively [19].

The weight loss of $Ba_{1-x}Sn_xTiO_3$ ($x = 0.00$, 0.02, 0.05, and 0.10) prepared by two different routes in each temperature range are summarized in Table 1. It can be seen that the weight loss of the sample from MSR was greater than that of SRR. It may be due to the difference in the microstructure, i.e., since the sample by MSR was quickly

Table 1 Weight loss of the samples for each temperature range

	~200 °C	200–800 °C	800 °C~
MSR			
$BaTiO_3$	1.4	2.7	0.3
$Ba_{0.98}Sn_{0.01}TiO_3$	1.4	2.8	0.6
$Ba_{0.95}Sn_{0.05}TiO_3$	1.8	3.1	0.8
$Ba_{0.90}Sn_{0.10}TiO_3$	2.3	3.0	0.6
SRR			
$BaTiO_3$	0.6	1.5	–
$Ba_{0.98}Sn_{0.01}TiO_3$	0.7	1.6	–
$Ba_{0.95}Sn_{0.05}TiO_3$	0.7	1.9	–
$Ba_{0.90}Sn_{0.10}TiO_3$	1.4	2.0	–

formed, it consisted of smaller particles with low crystallinity and might possess greater adsorption abilities of water and organic molecules than those by SSR. The weight loss of both the samples in the temperature range of 200–800 °C increased a little with an increase in the amount of Sn(II) added in the sample, indicating that the amount of OH group incorporated in the lattice increased with an increase in the amount of Sn(II). It is notable that the samples by MSR showed a little weight loss in the temperature range of 800–1000 °C, but the weight loss of the sample by SRR was negligibly small.

Crystal phases of samples

XRD patterns of the samples obtained by both MSR and SRR are shown in Figs. 3 and 4. It is seen that the samples prepared by SRR consisted of single perovskite phase, but a little diffraction peak around 24° corresponding to

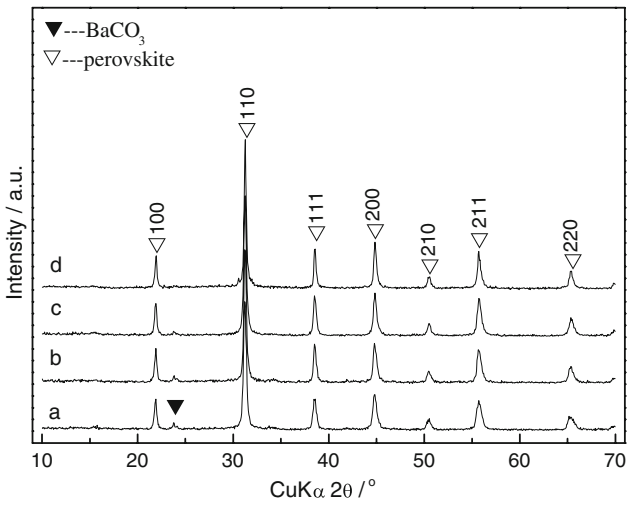

Fig. 3 XRD patterns for the (*a*) $BaTiO_3$, (*b*) $Ba_{0.98}Sn_{0.02}TiO_3$, (*c*) $Ba_{0.95}Sn_{0.05}TiO_3$, (*d*) $Ba_{0.90}Sn_{0.10}TiO_3$ powders as prepared by MSR at 200 °C for 1 h in 2-M KOH aqueous solutions

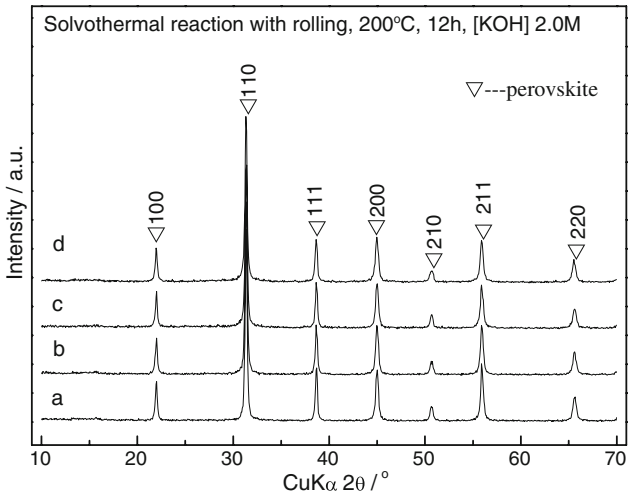

Fig. 4 XRD patterns for the (*a*) $BaTiO_3$, (*b*) $Ba_{0.98}Sn_{0.02}TiO_3$, (*c*) $Ba_{0.95}Sn_{0.05}TiO_3$, (*d*) $Ba_{0.90}Sn_{0.10}TiO_3$ powders as prepared by SRR at 200 °C for 12 h in 2-M KOH aqueous solutions

$BaCO_3$ appeared in the samples by MSR, which is consistent with the result of the TG-DTA analysis shown in Fig. 1.

Morphology of the powders

In a previous article [10], it was reported that the particle size of Sn^{2+}-doped barium titanate prepared by MSR increased, whereas the crystallinity decreased with an increase in the amount of doped Sn^{2+}. Similar profiles were also observed for Sn^{2+}-doped barium titanate prepared by SRR as shown in Fig. 5; although, the reasons of such change on the morphology and crystallinity of the grains were not clarified. One can suppose that the doped Sn^{2+} segregates at grain boundaries, which would decrease the crystallinity of the particles. It was also seen that the particle size of the samples prepared by MSR were smaller than that of SRR.

The sinterability

The samples were sintered at various temperatures for 5 h. Figure 6 shows the density of the sintered bodies from SRR as a function of the sintering temperature. The densities of all samples increased with an increase in sintering temperature up to 1200 °C, and then decreased probably due to the excess grain growth, which means that 1200 °C for 5 h was the optimum condition to sinter the present samples. It can be seen that the density decreased with an increase in the Sn^{2+} content. These results agreed with the TEM observations indicating that the crystallinity of the powder decreased with an increase in the Sn^{2+} content. The densities of the ceramic bodies sintered at 1200 °C for 5 h are

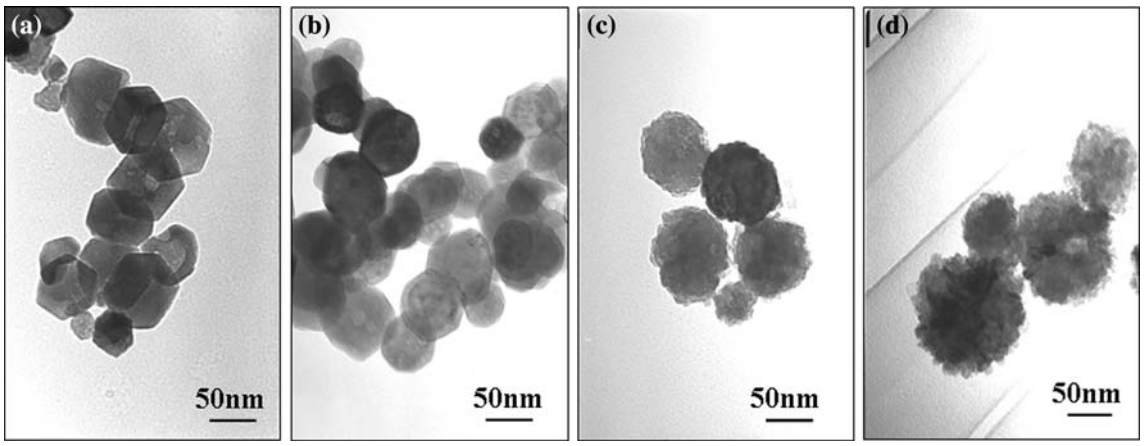

Fig. 5 SEM images of the **a** $BaTiO_3$ by MSR at 200 °C for 1 h, **b** $BaTiO_3$, **c** $Ba_{0.98}Sn_{0.02}TiO_3$, **d** $Ba_{0.95}Sn_{0.05}TiO_3$ by SRR at 200 °C for 12 h in 2-M KOH aqueous solutions

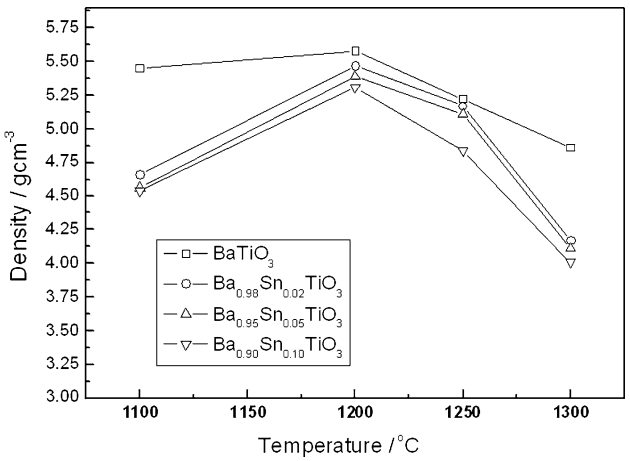

Fig. 6 The density of Sn^{2+}-doped $BaTiO_3$ sintered at various temperatures using the powders prepared by SRR at 200 °C for 12 h in 2-M KOH aqueous solutions

Table 2 The densities (g cm^{-3}) of the samples sintered at 1200 °C for 5 h

	MSR	SRR
$BaTiO_3$	5.44	5.58
$Ba_{0.98}Sn_{0.02}TiO_3$	5.35	5.47
$Ba_{0.95}Sn_{0.05}TiO_3$	5.32	5.39
$Ba_{0.90}Sn_{0.10}TiO_3$	5.20	5.31

tabulated in Table 2. The samples prepared by MSR showed a similar trend, and also lower sinterability than those of SRR.

Phase and morphology of ceramics body

Figures 7 and 8 show the XRD patterns of the sintered bodies of $BaTiO_3$, $Ba_{0.98}Sn_{0.02}TiO_3$, $Ba_{0.95}Sn_{0.05}TiO_3$, and $Ba_{0.90}Sn_{0.10}TiO_3$. All peaks could be attributed to the

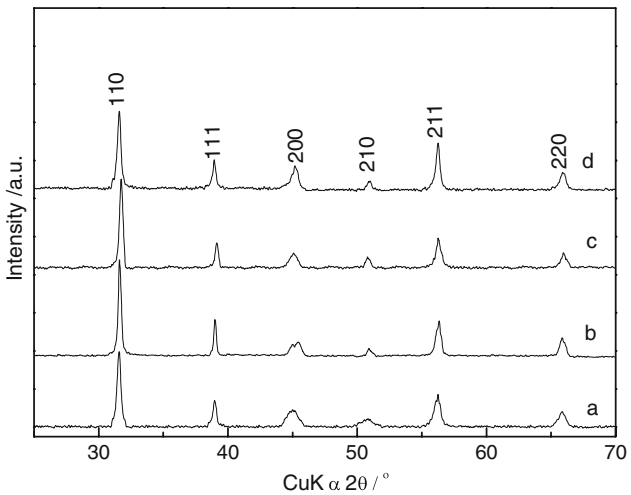

Fig. 7 XRD patterns of (*a*) $BaTiO_3$, (*b*) $Ba_{0.98}Sn_{0.02}TiO_3$, (*c*) $Ba_{0.95}Sn_{0.05}TiO_3$, (*d*) $Ba_{0.90}Sn_{0.10}TiO_3$ ceramics sintered at 1200 °C for 5 h using the powders obtained by MSR

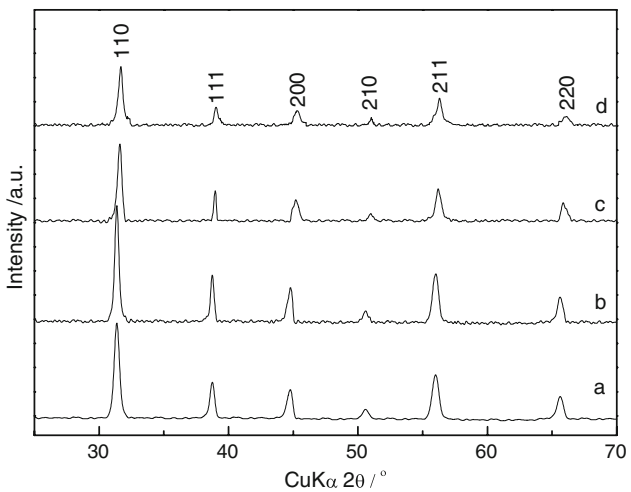

Fig. 8 XRD patterns of (*a*) $BaTiO_3$, (*b*) $Ba_{0.98}Sn_{0.02}TiO_3$, (*c*) $Ba_{0.95}Sn_{0.05}TiO_3$, (*d*) $Ba_{0.90}Sn_{0.10}TiO_3$ ceramics sintered at 1200 °C for 5 h using the powders obtained by SRR

Table 3 Lattice parameters, a (nm), of the samples

Sample	a_0(MSR)/nm		a_0(SRR)/nm	
	Powder	Sintered body	Powder	Sintered body
$BaTiO_3$	0.4037	0.4023	0.4031	0.4024
$Ba_{0.98}Sn_{0.02}TiO_3$	0.4036	0.4018	0.4025	0.4021
$Ba_{0.95}Sn_{0.05}TiO_3$	0.4033	0.4015	0.4022	0.4019
$Ba_{0.90}Sn_{0.10}TiO_3$	0.4031	0.4011	0.4021	0.4017

perovskite type $BaTiO_3$ and no other impurity phase appeared. Table 3 tabulated the lattice parameters of the prepared powders and sintered bodies. Compared with the powders, the lattice parameters of the sintered bodies decreased a little, probably due to the dehydration of OH^- in the lattice at high temperature. Furthermore, the splitting of the peak around 45° of 2θ indicating the existence of the tetragonal phase appeared for the sample $Ba_{0.98}Sn_{0.02}TiO_3$ by MSR (Fig. 7b).

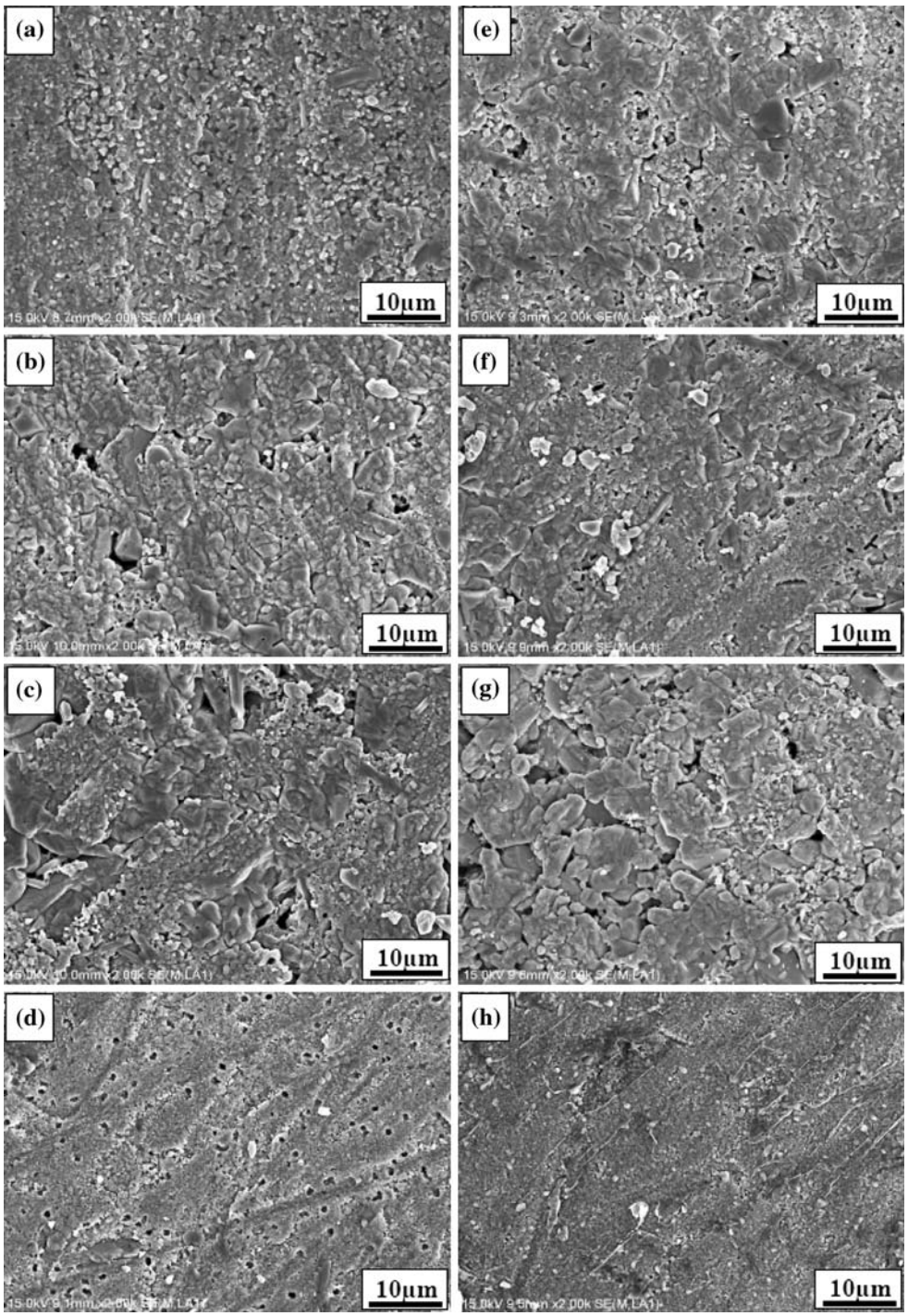

Fig. 9 SEM images of the fracture surfaces of samples sintered at 1200 °C for 5 h. **a** $BaTiO_3$, **b** $Ba_{0.98}Sn_{0.02}TiO_3$, **c** $Ba_{0.95}Sn_{0.05}TiO_3$, **d** $Ba_{0.90}Sn_{0.10}TiO_3$ by MSR at 200 °C for 1 h in 2-M KOH aqueous solutions, **e** $BaTiO_3$, **f** $Ba_{0.98}Sn_{0.02}TiO_3$, **g** $Ba_{0.95}Sn_{0.05}TiO_3$, **h** $Ba_{0.90}Sn_{0.10}TiO_3$ using the powders obtained by SRR at 200 °C for 12 h in 2-M KOH aqueous solutions

Figure 9 shows the scanning electron micrographs of the polished and thermal etched surfaces of the sintered bodies using the powders by MSR and SRR. The grain sizes of the samples by both MSR and SRR increased from 1 to 2 μm by doping with 2 and 5 mol% of Sn^{2+} ($x = 0.02$ and 0.05), but those doped with 10 mol% of Sn^{2+} ($X = 0.10$) decreased to less than 1 μm. These results suggest that the grain growth of $BaTiO_3$ is promoted by doping with small amount of Sn^{2+}, but excess amount of Sn^{2+} doping depressed the grain growth probably due to the segregation of tin oxide at the grain boundary.

Dielectric properties of sintering body

Figures 10 and 11 show the temperature dependence of relative dielectric constants and loss of $BaTiO_3$ with different Sn^{2+} contents at a frequency of 1 kHz. The undoped $BaTiO_3$ ceramic showed a Curie temperature, T_c, of 135 °C as reported, but the addition of a small amount of Sn^{2+} resulted in the decrease of the Curie temperature to 130, 125, and 120 °C for $x = 0.02$, 0.05, and 0.10, respectively. Generally, it is accepted that the microstructure, especially the grain size, has a significant effect on the dielectric property, and a smaller the grain size can improve the dielectric constant at room temperature [20–22]. Present results suggest that an increase in the Sn^{2+} content results in an increase in the grain size and decrease in the dielectric constant below the Curie temperature. However, the Curie temperature also decreases with increase in the Sn^{2+} content, indicating that the Curie temperature is more strongly influenced by the Sn^{2+} content than the grain size. But at Curie temperature, the value of the dielectric peak is larger for the sample with a larger grain size due to the "grain size effects" [23–25].

The samples obtained by MSR exhibited lower dielectric loss than those obtained by SRR. The values reached a minimum around the Curie temperature, and then increased above 225 °C. In both the cases, the samples with $x = 0.2$ and 0.5 showed relatively higher values of dielectric loss, which may be concerned with the increase in a second phase at the grain boundary. There is a possibility that Sn^{2+} was partly oxidized to form $BaTi_{1-x}Sn_xO_3$ during the sintering, which may affect the dielectric properties. The details are now under investigation.

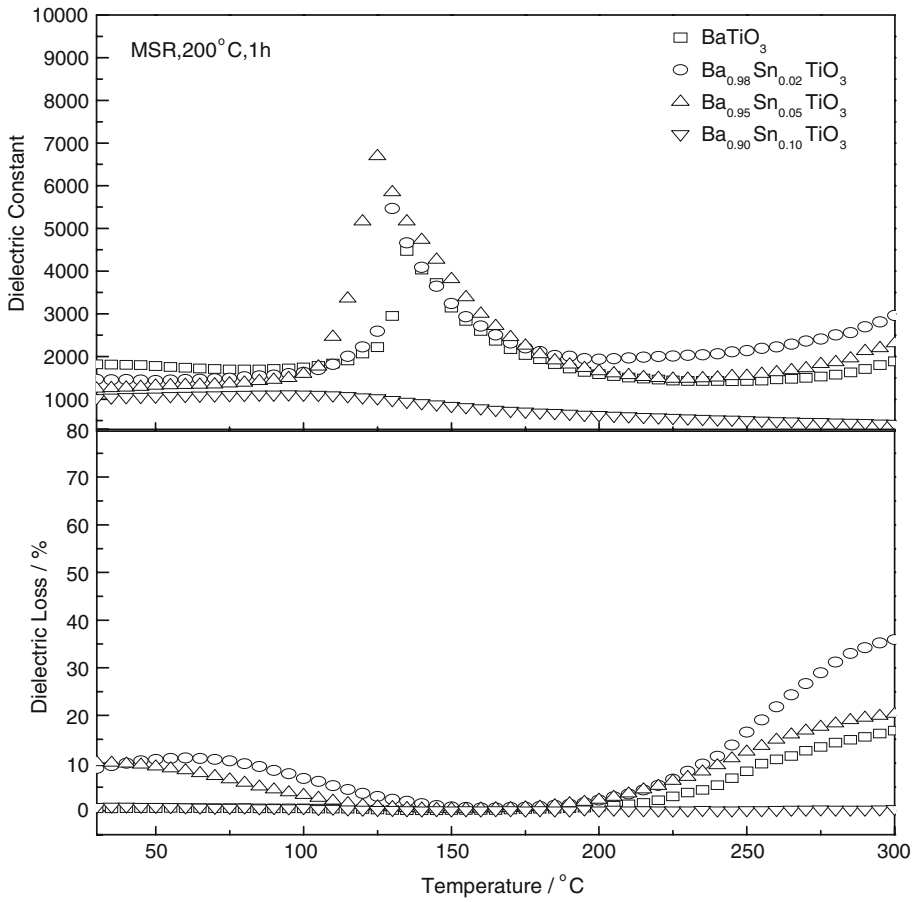

Fig. 10 Dielectric constants and dielectric loss of $Ba_{1-x}Sn_xTiO_3$ ($x = 0$, 0.02, 0.05, and 0.10) sintered bodies using the powders by MSR at 200 °C for 1 h

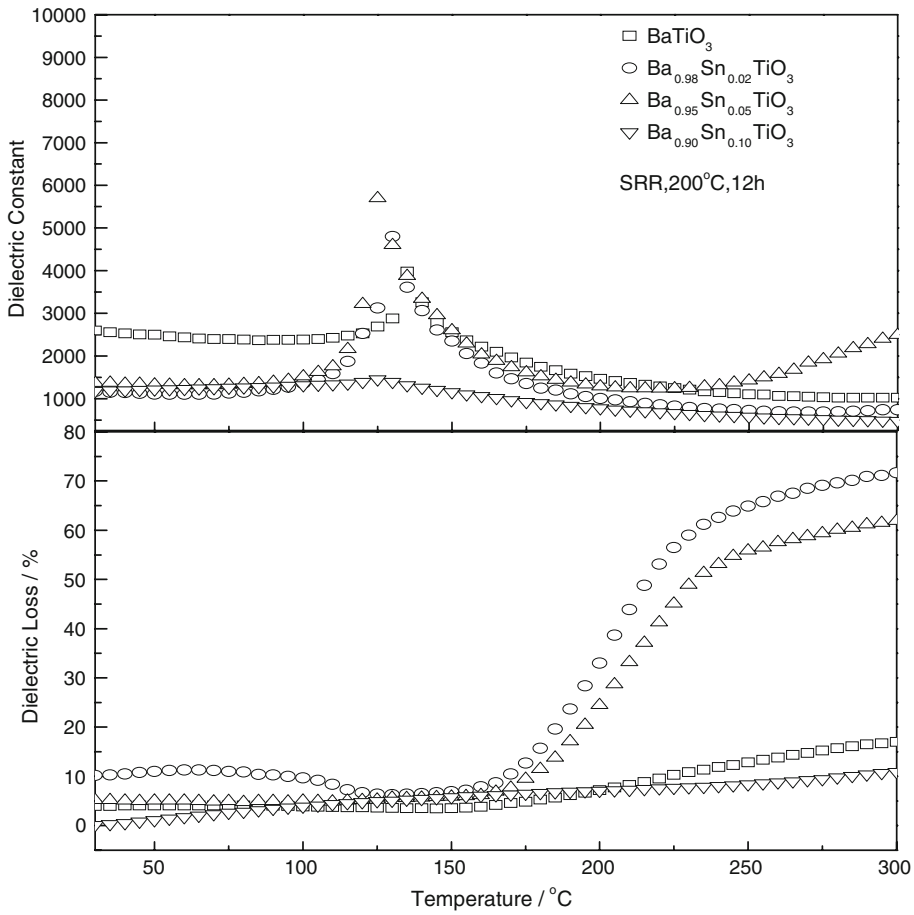

Fig. 11 Dielectric constants and dielectric loss of $Ba_{1-x}Sn_xTiO_3$ ($x = 0$, 0.02, 0.05, and 0.10) sintered bodies using the powders by SRR at 200 °C for 12 h

Conclusion

Nanoparticles of Sn^{2+}-doped $BaTiO_3$ were obtained as a single perovskite phase using both MSR and SRR at a moderate temperature such as 200 °C. From the changes in the various properties obtained by doping with Sn^{2+}, it was confirmed that the Sn^{2+} entered into the lattice of the $BaTiO_3$. A small amount of Sn^{2+} doped in the $BaTiO_3$ ($x \leq 0.05$) led to the increase in the grain size of the sintered body and decrease in the Curie temperature and dielectric constant below Curie temperature. However, doping with excess amount of Sn^{2+} led to a decrease in the sinterability.

Acknowledgements This research was partially supported by the Ministry of Education, Culture, Sports, Science and Technology, "Special Education and Research Expenses, Post-Silicon Materials and Devices Research Alliance".

References

1. Hosogi Y, Shimodaira Y, Kato H, Kobayashi H, Kudo A (2008) Chem Mater 20:1299. doi:10.1021/cm071588c
2. Mizoguchi H, Wattiaux A, Kykyneshi R, Tate J, Sleight AW, Subramanian MA (2008) Mater Res Bull 43:1943. doi:10.1016/j.materresbull.2008.03.011
3. Konishi Y, Ohsawa M, Yonezawa Y, Tanimura Y, Chikyow T, Wakisaka T, Koinuma H, Miyamoto A, Kubo M, Sasata K (2003) Mater Res Soc Symp Proc 748:U3.13.1
4. Hosogi Y, Tanabe K, Kato H, Kobayashi H, Kudo A (2004) Chem Lett 33:28. doi:10.1246/cl.2004.28
5. Konisi Y, Osawa M, Yonezawa Y (2003) Fuji Jiho 76(4):241 in Japanese
6. Jeitschko W, Sleight AW (1974) Acta Crystallogr Cryst Chem B30:2088. doi:10.1107/S0567740874006534
7. Ercit TS, Cerny P (1988) Can Mineral 26:899
8. Kumada N, Yonesaki Y, Takei T, Kinomura N, Wada S (2009) Mater Res Bull 44:1298. doi:10.1016/j.materresbull.2008.12.017
9. Xie YH, Yin S, Yamane H, Hashimoto T, Machida H, Sato T (2008) Chem Mater 20:4931. doi:10.1021/cm800277b
10. Xie YH, Yin S, Hashimoto T, Kimura H, Sato T (2009) J Mater Sci 44:4834. doi:10.1007/s10853-009-3737-8
11. Polla DL, Lorraine FF (1998) Ann Rev Mater Sci 28:563. doi:10.1146/annurev.matsci.28.1.563
12. Takenaka T, Nagata H (2005) J Eur Ceram Soc 25:2693. doi:10.1016/j.jeurceramsoc.2005.03.125
13. Mark AM, Elliott BS (2003) J Eur Ceram Soc 23:2143. doi:10.1016/S0955-2219(03)00022-0
14. Xinhua Z, Jianmin Z, Shunhua Z, Zhiguo L, Naiben M, Dietrich H (2005) J Cryst Growth 283:553. doi:10.1016/j.jcrysgro.2005.05.080
15. Zhonghua Y, Hanxing L, Yan L, Zhaohui W, Zongyang S, Yang L, Minghe C (2008) Mater Chem Phys 109:475. doi:10.1016/j.matchemphys2007.12.019
16. Rath MK, Pradhan GK, Pandey B, Verma HC, Roul BK, Anand S (2008) Mater Lett 62:2136. doi:10.1016/j.matlet.2007.11.033

17. Yong-Il K, Kwon-Sang R, Seung-Hoon N, Jong-Seo P (2006) Curr Appl Phys 6S1:e266. doi:10.1016/j.cap.2006.01.053
18. Yuji H, Kiyoka T, Cihangir D, Kimiysu S, Takaaki N, Koji W (2008) Mater Sci Eng A 475:57. doi:org/10.1016/j.msea.2006.12.138
19. Srimala S, Ahmad FMN, Zainal AA, Radzali O, Anthony W (2008) J Mater Process Technol 195:171. doi:org/10.1016/j.jmatprotec.2007.04.120
20. Hosseini M, Moosavi SJ (2000) Ceram Int 26:541. doi:10.1016/S0272-8842(99)00092-9
21. Wang YG, Zhong WL, Zhang PL (1994) Solid State Commun 92(6):519. doi:0038-1098(94)00498-6
22. Arlt G, Hennings D, de With G (1985) J Appl Phys 58(4):1619
23. Lin S, Lü T, Jin C, Wang X (2006) Phys Rev B 74:134115
24. Zhao Z, Buscaglia V, Viviani M, Buscaglia MT, Mitoseriu L, Testino A, Nygren M, Johnsson M, Nanni P (2004) Phys Rev B 70:024107. doi:10.1103/PhysRevB.70.024107
25. Subbarao EC (1998) Colloids Surf A 133:3. doi:10.1016/S0927-7757(97)00104-0